ACS APPLIED MATERIALS & INTERFACES

Research Article

www.acsami.org

Improving the Performance of Titania Nanotube Battery Materials by Surface Modification with Lithium Phosphate

María C. López, Gregorio F. Ortiz,* José R. González, Ricardo Alcántara, and José L. Tirado

Laboratorio de Química Inorgánica, Universidad de Córdoba, Edificio Marie Curie, Campus de Rabanales, 14071 Córdoba, Spain

Supporting Information

ABSTRACT: Self-organized TiO_2 nanotubes ranging from amorphous to anatase structures were obtained by anodization procedures and thermal treatments at 500°C. Then electrolytic Li_3PO_4 films were successfully deposited on the nanotube array by an electrochemical procedure consisting in proton reduction with subsequent increase in pH, hydrogen phosphate dissociation and Li_3PO_4 deposition on the surface of the cathode. The Li_3PO_4 polymorph (γ or β) in the deposit could be tailored by modifying the electrodeposition parameters, such as time or current density, as determined by X-ray patterns. The morphological analysis evidenced the formation of a 3D nanostructure consisting of Li_3PO_4 coating the TiO_2 nanotube array. The anode−solid electrolyte stacking was tested in lithium half cells. Interestingly, the electrochemical performances revealed a better cycling stability for samples containing low amount of lithium phosphate, which is deposited for short times and low current densities. These results suggested the possibility of fabricating 3D Li-ion batteries. nt-TiO_2/γ-Li_3PO_4/$LiFePO_4$ full cells were cycled at different rates in the C/5-5C range. This cathode-limited microbattery delivered a reversible gravimetric capacity of 110 mA h g^{-1} and a capacity retention of 75 % after 190 cycles at 5C.

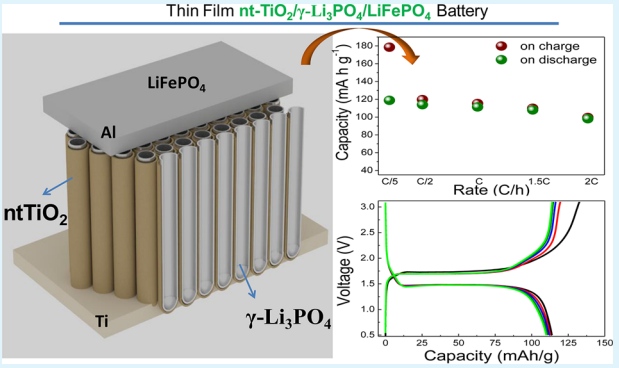

KEYWORDS: *lithium phosphate, titania nanotubes, anodization, electrodeposition, microbatteries*

INTRODUCTION

Solid electrolyte interfaces are crucial for the performance of lithium-ion batteries.[1,2] The formation of a surface layer on the electrodes of usual Li-ion arrangements takes place by irreversible reactions with the electrolyte. An alternative approach is to coat the electrodes with a convenient ionic conductor that warrants lithium ion diffusion from the electrolyte or acts as a solid electrolyte itself. Thin film electrodes, such as TiO_2 nanostructured films obtained by Ti anodization, are particularly suitable to this approach, as shown in this study.

Titanium dioxide has attracted a great interest for the fabrication of new electrochemical accumulators especially as active electrode material for Li-ion batteries.[3,4] TiO_2 is a promising alternative to conventional anodes, because it can operate at high voltages (~1.7 V vs Li^+/Li) which provide enhanced safety as compared with carbon-based electrodes (~0.1 V vs Li^+ (1M)/Li). Thus, a titania-based anode reduces the overall cell voltage but provides cells with good capacity retention on cycling and low self-discharge. When prepared in the form a thin layer of self-organized nanotubes[5,6] not only the specific surface area for reacting with lithium significantly increases but also the accommodation of other electroactive species is possible.[7,8] The compound Li_3PO_4 is known to be a potential candidate for thin film lithium electrolyte.[9] The solid is permeable to lithium ions and impermeable to electrons, and has light weight and wide potential range of stability vs lithium. Also, lithium *o*-phosphate can be used in thin films due to its thermal and mechanical stability.[10,11]

The olivine-related $LiFePO_4$ is now firmly established as a convenient cathode material in Li-ion batteries. It has good cycle stability, a high theoretical specific capacity of 170 mAh g^{-1}, and a flat discharge potential plateau of 3.4 V vs Li/Li^+. However, the widespread use of $LiFePO_4$ as battery cathodes is limited by its poor rate capability caused by its intrinsic low electronic conductivity and slow diffusion rate of lithium ions.[12,13]

The present work is focused on the improvement of a self-organized anatase nanotube electrode by protecting the surface with a deposit of lithium phosphate ionic conductor. For this purpose, the fabrication of lithium phosphate thin film onto self-organized TiO_2 nanotube layers ($ntTiO_2$) is carried out as a previous step before combining with $LiFePO_4$ that was obtained under similar conditions to those in ref 14. The scientific approach is to improve the electronic and ionic conductivity of materials taking the benefits that an inexpensive method like electrochemical-based procedures may offer. The effects of Li_3PO_4 thickness on the electrochemical perform-

Received: January 10, 2014
Accepted: March 31, 2014
Published: March 31, 2014

   dx.doi.org/10.1021/am500189h | ACS Appl. Mater. Interfaces 2014, 6, 5669−5678

ances are reasonably explained. Also, the experimental studies intend to show a way of fabricating low crystalline and amorphous materials into the electrode to increase the interphase area between the active materials and the electrolyte which is for sure beneficial for prolonged cycling. Previous studies found how to improve the interface resistivity as well as the mechanical stability.[15,16] An example of an all-solid-state Li/Li_3PO_4/$LiCoO_2$ battery was fabricated by using pulsed laser deposition (PLD) grown-up Li_3PO_4 thin films and showed excellent intercalation properties and electrochemical stability in the operating voltage range from 0 to 4.7 V vs Li^+/Li^0.[17] The latest advancements in micro- and nano-electromechanical systems (MEMS/NEMS) technology have conducted to multiple small-scale devices in microelectronics and biomedical area including microsensors or drug delivery systems. Consequently, it is mandatory to develop small-scale electrical power sources that make possible delivery of power in these microscale devices. Here, the electrochemical performance of a rocking chair TiO_2/Li_3PO_4 ($LiPF_6$ in EC:DEC)/$LiFePO_4$ microbattery is shown. We think that the proposed microbattery could be suitable for such low voltage (<2.0 V) applications.

EXPERIMENTAL MATERIALS AND METHODS

The fabrication of self organized titania nanotubes ($ntTiO_2$) is carried out through an anodization process in a cell that consists of Ti foil (0.127 mm thick, 99.7 % purity) and Pt wire as a working electrode and counter electrode, respectively. A 0.3 wt % solution of NH_4F in ethylenglycol (EG)/water (92:8 vol) mixture was used as electrolyte.[18] The experiments consisted of applying a constant voltage of 60 V during 120 min using a voltage source (Agilent B2912A).

To have comparative results, the deposition of electrolytic Li_3PO_4 was performed in three different substrates: Ti foils, amorphous $ntTiO_2$ obtained at room temperature (RT) and crystalline anatase $ntTiO_2$ at 500°C. The deposition bath consisted of 0.5 M $LiNO_3$ and 0.02 M $NH_4H_2PO_4$ mixed in aqueous solution. Electrolytic Li_3PO_4 films were deposited by an electrochemical procedure consisting in proton reduction with subsequent local increase of pH in the vicinity of the substrate surface, hydrogen phosphate dissociation and Li_3PO_4 deposition on the surface of the cathode.[11] The electrodeposition was carried out at room temperature (RT), using a potentiodynamic method with −1 V potential. Additionally, the galvanostatic method was extensively employed using current densities in the 3.75−75 mA cm^{-2} (vs. Ag/AgCl) range and deposition times from 1 to 40 min with an Arbin Galvanostat/Potentiostat apparatus. The 0.65 cm^2 $ntTiO_2$-based substrates served as working electrode, a platinum wire as the counter electrode and saturated Ag/AgCl as reference electrode. Additionally, the as-prepared coated specimens were further calcined for 3 h at 500°C (referred as anodized-deposited-calcined, ADC) to induce the formation of γ-Li_3PO_4. The electrodeposition of β-Li_3PO_4 on crystalline $ntTiO_2$ was also performed (referred as anodized-calcined-deposited ACD).

The crystal structures of the as-deposited and calcined Li_3PO_4-$ntTiO_2$-based films were analyzed by X-ray diffraction (XRD) in a D5000 Siemens diffractometer (CuKα radiation) operating at 40 kV voltage and a current of 30 mA. Grazing-incidence small-angle X-ray diffraction (GISAXRD) patterns were obtained in an EQ 31 04 Panalytical X'Pert PRO MPD system equipped with Cu Kα radiation. The morphology and composition of the prepared electrode materials was examined in a JEOL SM6300 Scanning Electron Microscopy (SEM) instrument equipped with Energy-Dispersive X-ray Spectroscopy (EDS) microanalysis and in a Philips CM10 Transmission Electron Microscopy (TEM) instrument. The X-ray Photoelectron Spectroscopy (XPS) measurements are performed in a SPECS Phobios 150MCD instrument using Mg Kα source (1253.6 eV) and chamber pressure of 4×10^{-9} mbar. The C 1s peak at 284.9 eV of adventitious carbon was used as reference.

AC impedance spectroscopy was performed in a AUTOLAB PGSTAT-12, The Ti/Li_3PO_4-based films are used as the working electrode, lithium metal as the counter and reference electrode in 1M $LiPF_6$ in 1:1 (v/v) EC-DMC solution as the liquid electrolyte. The assemblage of cells was conducted in an argon-filled glove box (M. Braun). The total conductivity is determined using $\sigma = (L/A)/R_b$, where A is the area contact (0.7854 cm^{-2}), L is the film thickness of the pellet or the thin film, and R_b the resistance.

The electrochemical characterization and cycling properties (discharge−charge) were performed using a Biologic-VMP instrument. The lithium cells (Swagelok-type) were assembled in a drybox under Ar atmosphere. A 9 mm in diameter lithium disk was used as negative electrode, and Li_3PO_4−$ntTiO_2$-based films were used as positive electrode. For the rocking chair battery the following configuration was used: TiO_2/Li_3PO_4 ($LiPF_6$ in EC:DEC)/$LiFePO_4$, which was cycled at different rates: C/10, C/5, C/2, C, 2C, and 5C between 0.5−3.1 V.

RESULTS AND DISCUSSION

After the deposition of electrolytic lithium phosphate by potentiostatic method at −1.0 V (Ag/AgCl) for 20 min, no peaks were detected in the X-ray diffraction patterns (Figure 1),

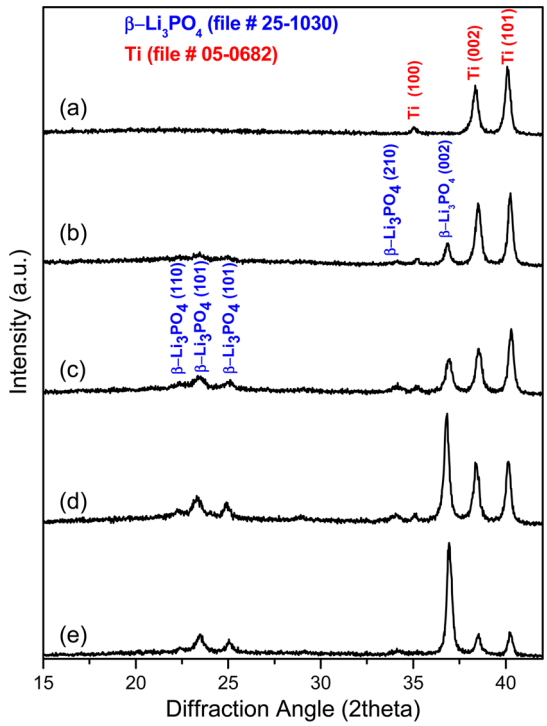

Figure 1. XRD patterns of the as-deposited Li_3PO_4 films under potentiostatic and galvanostatic regime at (a) −1 V and 20 min, (b) −150 mA cm^{-2} and 10 min, (c) −75 mA cm^{-2} and 20 min, (d) −75 mA cm^{-2} and 30 min, and (e) −75 mA cm^{-2} and 40 min.

thus showing a poorly crystalline character of the lithium phosphate deposits on Ti. Using the galvanostatic method described in the experimental section, crystalline β-Li_3PO_4 phase (JCPDS 25-1030) was successfully deposited on Ti-based substrates, as shown by X-ray diffraction (Figure 1). The β-Li_3PO_4 coated film had different crystallite size depending on time and current density of the deposition process. The average crystallite size was estimated using the Scherrer equation for (002) peaks placed at about 37° (2θ). The crystallite size oscillated between 200 and 300 Å for 10 to 40 min of electrodeposition, respectively. Clearly, the preferred growth

dx.doi.org/10.1021/am500189h | ACS Appl. Mater. Interfaces 2014, 6, 5669−5678

orientation of β-Li_3PO_4 crystallites can be identified by the higher intensity ratio between the (002) and (101) reflections (Figure 1b–e). By simple calcination at 500°C in air, the β-Li_3PO_4 specimen can be transformed into γ-Li_3PO_4 (JCPDS 15-0760) as shown in Supporting Information Figure S.I.1. From the pattern no obvious differences between the strong peaks of β-phase (110), (101), and (210) and γ-phase (120), (101,) and (220) are observed, but from the fitting with *fullprof* software a notable difference in the unit cell parameter could be discerned for both phases. The unit cell parameters were calculated and resulted to be very close to those reported in literature for pure samples (see Table 1 in Supporting Information).[19,20]

To form thinner Li_3PO_4 films or finely disperse the phosphate into $ntTiO_2$ arrays, it was necessary to use low current density and short deposition time. Hence, the crystalline character of the deposits may change drastically under such conditions. The crystalline character of Li_3PO_4 was lost when deposition time was decreased from 20 to 1 min, and also when current density decreased from 37.5 to 3.75 mA cm^{-2} as shown by X-ray diffraction (see Supporting Information Figure S.I.2). This effect was not only observed for samples obtained at room temperature but also for those samples that were calcined at 500 °C either before or after electrolytic Li_3PO_4 deposition (see Supporting Information Figure S.I.3 and S.I.4). To determine the presence of lithium phosphate on the $ntTiO_2$ surface SEM, EDS, GISAXRD and XPS were performed. In addition, the electrochemical properties are analyzed in Li cells, which were very helpful to observe changes in the cycling behavior as compared with the Li_3PO_4-free $ntTiO_2$ electrode.

One of the most important characteristic of solid electrolyte materials is the ionic conductivity. Here, the compatibility of lithium phosphate with TiO_2 is important to be resolved. So, the impedance spectra for our synthesized lithium phosphate is compared to that from commercial source (Aldrich) and plotted in the Nyquist complex plane (Figure 2). The equivalent circuit used for fitting is represented as R_s(CPE-((R_b)(W))). The semicircle observed at high frequencies represents the bulk resistance of the studied material denoted with R_b. The equivalent circuit used for the fitting is based on a parallel combination of bulk resistance (R_b) and constant phase element (CPE). The resistance R_s represents the resistance of the overall electrical measurement system which is in series with the R_b and CPE. The bulk resistance includes both the grain interior resistance and the grain boundary resistance. These two components cannot be easily separated in all samples as observed from the spectra. At low frequencies, an inclined line is observed which approximately 45° angle to the real axis, denoted as Warburg impedance.[21] The conductivity of our electrodeposited Li_3PO_4 material is about 1.5×10^{-5} S cm^{-1} while for commercial products 8.2×10^{-7} S cm^{-1} is obtained. Typical conductivities found in the literature are 8.6×10^{-8} S cm^{-1} for β-Li_3PO_4 prepared by electrodeposition on Pt and calcined at 300 °C K, and 7×10^{-8} S cm^{-1} for Li_3PO_4 deposited by sputtering in Ar + O_2 atmosphere.[11,22] These values are in agreement with the conductivities reported here. Although higher bulk conductivities are preferred for practical solid electrolytes, an improvement in the electrochemical behavior of nt-TiO_2 by electrodeposition of Li_3PO_4 thin films on the surface of the electrode will be demonstrated below.

A representative view of SEM images of anodized $ntTiO_2$, electroplated Li_3PO_4 on Ti foils and Li_3PO_4 on $ntTiO_2$ are

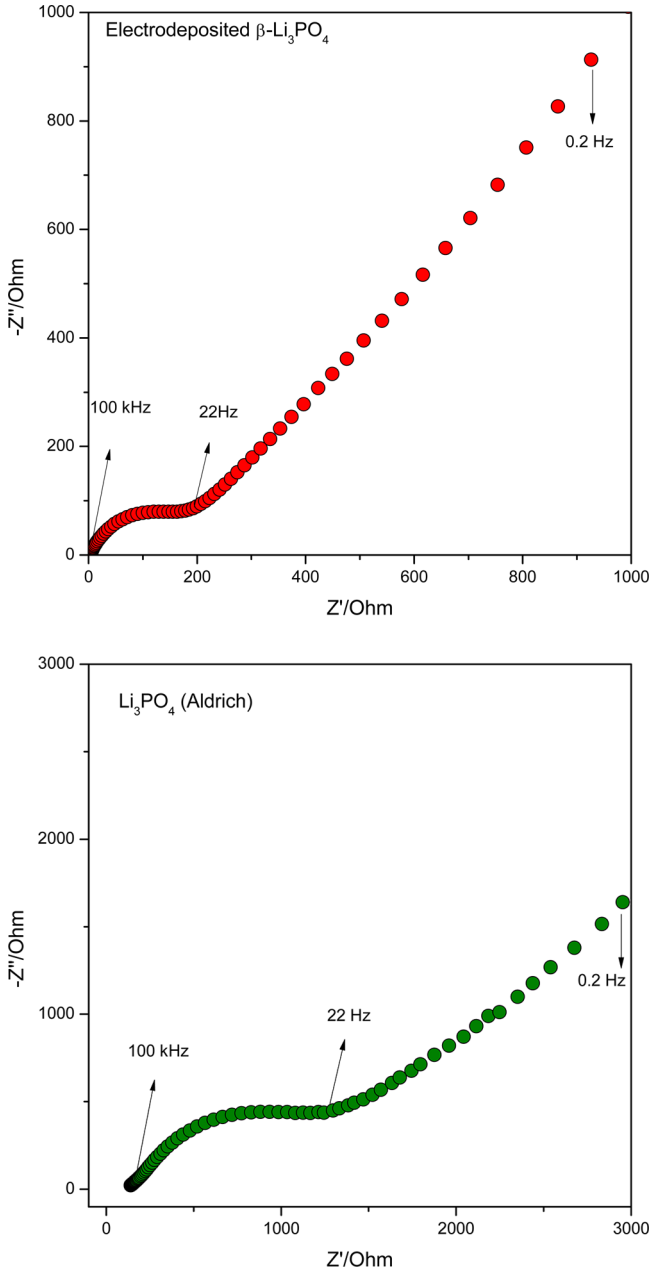

Figure 2. Impedance spectra of our electroplated thin film-based lithium phosphate compared to commercial Li_3PO_4 (Aldrich).

shown in Figures 3 and 4 and Supporting Information Figure S.I.5. Firstly, the as-prepared $ntTiO_2$ at R.T. at 60 V and 2 h presented about 8.5-10 μm of tube length and about 50–60 nm of tube diameter as deduced from SEM and TEM (inset of Figure 3a and b) images. It is worth noting that nanotube morphology did not present any changes when a thermal calcination at 500 °C is carried out. However, the crystalline character changed to anatase phase, as observed from the (101), (004), (200), (105), and (211) reflections (Supporting Information Figures S.I.3 and S.I.4). From our own previous experience, not only the amorphous but also the crystalline anatase $ntTiO_2$ thin films grown on the metallic Ti foil is mechanically robust enough to be used as the anode directly in the final battery.[5–8,18] The idea is to demonstrate here that they are also valid for supporting the stacking $ntTiO_2$/Li_3PO_4 as well as was previously demonstrated an enhanced electrochemical

dx.doi.org/10.1021/am500189h | ACS Appl. Mater. Interfaces 2014, 6, 5669–5678

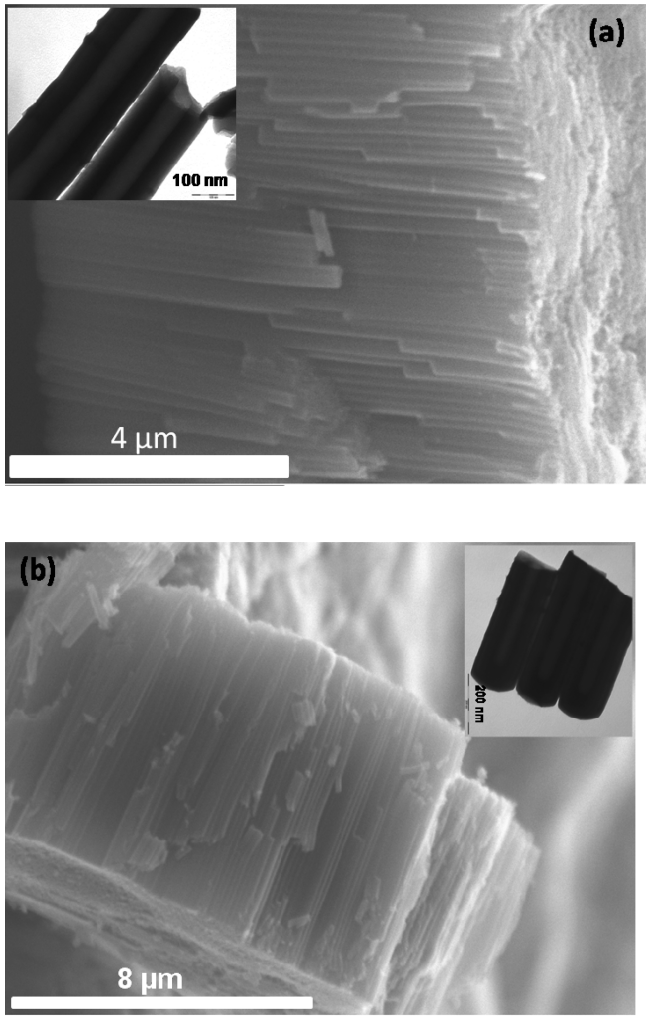

Figure 3. SEM images of $ntTiO_2$ fabricated by anodization at 60 V during 2 h at (a) RT and (b) calcined at 500 °C. The insets show a detailed view of the nanotubes.

behavior in lithium batteries of self-organized titanium dioxide nanotubes by surface polyacrylonitrile electropolymerization.[23] Such electrode designs are expected to offer marked improvements in power while maintaining comparable energy density and could be understood as an imposed prerequisite to future fabricate small-scale batteries. Indeed, possibly high Li ionic diffusion rates make the lithiation of $ntTiO_2$ nanotubes much easier as found in lithium tin phosphates on with is formed Li_3PO_4 in situ.[24]

A deep insight on the morphology of Li_3PO_4 deposits on $ntTiO_2$ with several examples is shown. A compact β-Li_3PO_4 thin film of about 6−6.5 μm on Ti-foils is obtained at 37.5 mA cm^{-2} during 20 min (Supporting Information Figure S.I.5a). For higher times ∼30 min morphological changes of the deposits are observed, appearing agglomeration of some spheres onto the layer (Supporting Information Figure S.I.5c). The morphology of electrodeposited Li_3PO_4 changed drastically when performed on the self-organized $ntTiO_2$ layer. For instance, after 20 min of deposition time, the surface is completely covered by large Li_3PO_4 particles (Supporting Information Figure S.I.5d). This over 20 μm thick layer would not be beneficial for such cycling purposes as electrodes in batteries. The changes in morphology and crystallinity are more evident when scaling down to nanometric size in fabrication

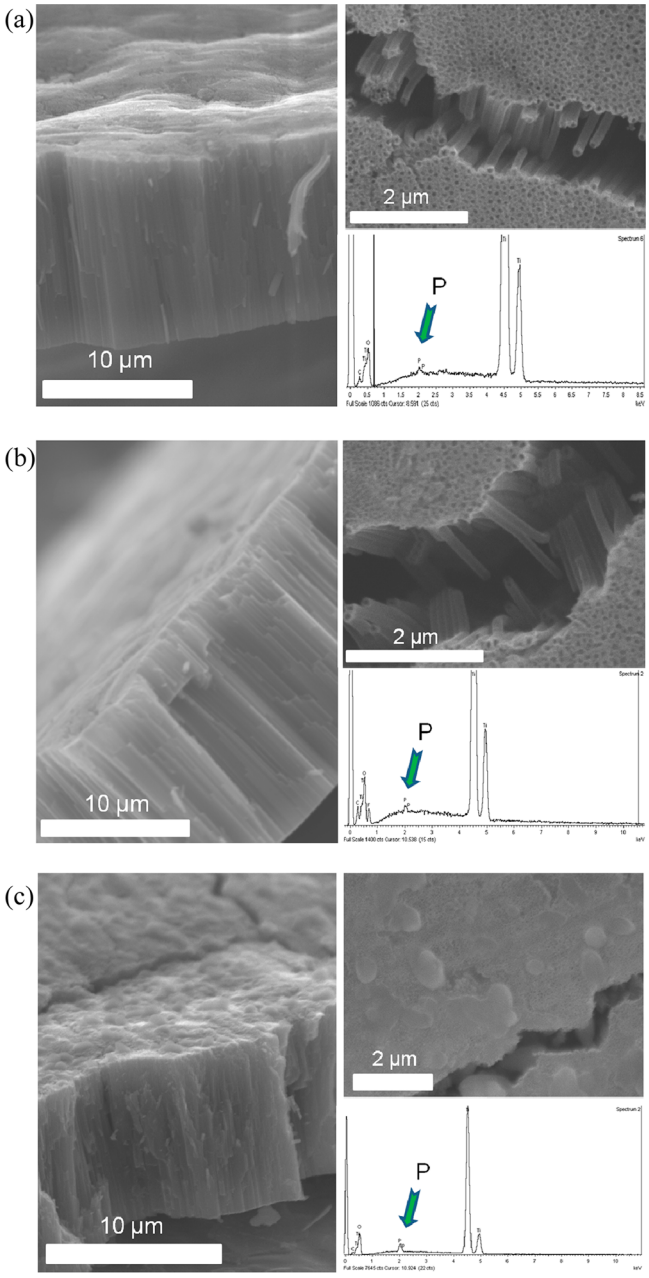

Figure 4. SEM images and EDS of $ntTiO_2$ with electrodeposited Li_3PO_4 under different conditions: (a) on crystalline $ntTiO_2$ using 1 min and 3.75 mA cm^{-2}, (b) on amorphous $ntTiO_2$ using 1 min and 3.75 mA cm^{-2}, and (c) on crystalline $ntTiO_2$ using 1 min and 37.5 mA cm^{-2}.

procedure, particularly a more homogeneous deposit is obtained. The SEM images of the Li_3PO_4-coated $ntTiO_2$ with different current density (3.75 and 37.5 $mAcm^{-2}$) are displayed in Figure 4. The covering effect of Li_3PO_4 can be observed for 1 min of electrodeposition at 37.5 mA cm^{-2} as the nanotubes are filled (Figure 4c). As compared to the SEM image of the as-prepared $ntTiO_2$ shown in Figure 3a which reveals thin tube walls (by TEM around 50 nm) and tube diameter (around 50 nm) the sample in Figure 4c presents some degree of perforation at the top. As the current density decreases around ten times (e.g., 3.75 mA cm^{-2}), the $ntTiO_2$ surface is not clearly covered by Li_3PO_4 as observed by SEM. However, the EDS analyses revealed the presence of P atoms in the TiO_2 array. It

dx.doi.org/10.1021/am500189h | ACS Appl. Mater. Interfaces 2014, 6, 5669−5678

can as well be noticed that the perforation in the tube walls has clearly disappeared (Figure 4a,b). These results could be indicative that the growth of Li_3PO_4 occurred on the inside of nanotube wall not only for samples obtained at room temperature (β-Li_3PO_4) but also for that obtained at 500°C (γ-Li_3PO_4), see Figure 4a and b.

To get further insight of these samples, analyses by GISARXD and XPS are performed. The grazing incident scans from 0.3° ω (the incidence angle) to 1.0° ω each 0.1° scans were made to detect Li_3PO_4 (Supporting Information Figure S.I.6). No peaks of Li_3PO_4 could be detected (most intense peak at $2\theta = 22.3°$), only the peak of anatase which was identified by HighScore software (see Supporting Information Figure S.I.7). There is no indication that the β-Li_3PO_4 is amorphous, because the background does not show any indication of amorphous bands on the position where the Li_3PO_4 peaks could be expected. Most probably, the ntTiO_2 coating array quantity is not detected in such small amount. X-ray photoelectron spectra of P 2p, Ti 2p, and O 1s were measured and shown in Figure 5. First, it should be noted that the surface chemical composition of the different thin films is in agreement with the chemical compositions determined by XRD patterns and EDS analyses, these two techniques allowing an in-depth analysis of the samples. The P $2p_{3/2}$ XPS region shows a simple signal appearing at a maximum of 133 eV that can be attributed to two overlapping signals due to P atoms with oxygen atoms that are singly (P−O−P) or doubly (P═O) bonded in Li_3PO_4. Apparently, as in the case of MPO_4, this signal is consequently assigned to phosphate anions.[25,26] The peaks ascribable to Ti2 $p_{3/2}$ and Ti $2p_{1/2}$ emerged at around 458.9 and 464.6 eV, respectively (Fig. 5) which agree very well with data reported in the literature.[27] The O 1s signal at 530.2 and 534.9 eV was identified as oxygen in TiO_2 and in Li_3PO_4, respectively (Fig. 5c). Although the position of O 1s peaks are slightly shifted to higher binding energies as compared to that observed in LIPON,[28] the main O 1s peak attributed to Li_3PO_4 can be decomposed into three components: (i) P═O (non-bridging oxygen at 532.9 eV), (ii) Li^+−O−P (non-bridging oxygen at 534.9 eV), and (iii) P−O−P (bridging oxygen at 536.9 eV). The cations around the PO_4 cluster and the distortion of the PO_4 tetrahedra because of the anisotropic crystal forces play a minor role and their influence on the valence band spectra was found to be negligible.[29] To evaluate if lithium phosphate is inside the ntTiO_2, Ar^+-etching is performed during 20 and 50 min. Consequently, a decreasing in the intensity peaks of Ti 2p and P 2p are observed in the same proportion, entailing that such composition is homogeneous along the ntTiO_2 array (Supporting Information Figure S.I.8). Moreover, EDS mapping revealed that P atoms are uniformly dispersed on ntTiO_2 array within the resolution of the used apparatus (Supporting Information Figure S.I.11).

The effect of lithium phosphate (β- and γ-Li_3PO_4) on the electrochemical performance of amorphous and crystalline ntTiO_2 is presented next. Galvanostatic charge and discharge tests using a current density of 50 μA cm^{-2} and using two different voltage windows were carried out: (i) 0.05−3.0 V and (ii) 1.0−3.0 V (vs Li^+/Li^0). Depending on the area of the ntTiO_2 array used as electrode the areal capacity will vary, that is the reason for always using 0.65 cm^2 electrodes in our experiments. Although areal capacities are important for microbattery applications, volumetric or gravimetric capacities are mandatory to compare with literature results. Therefore, the

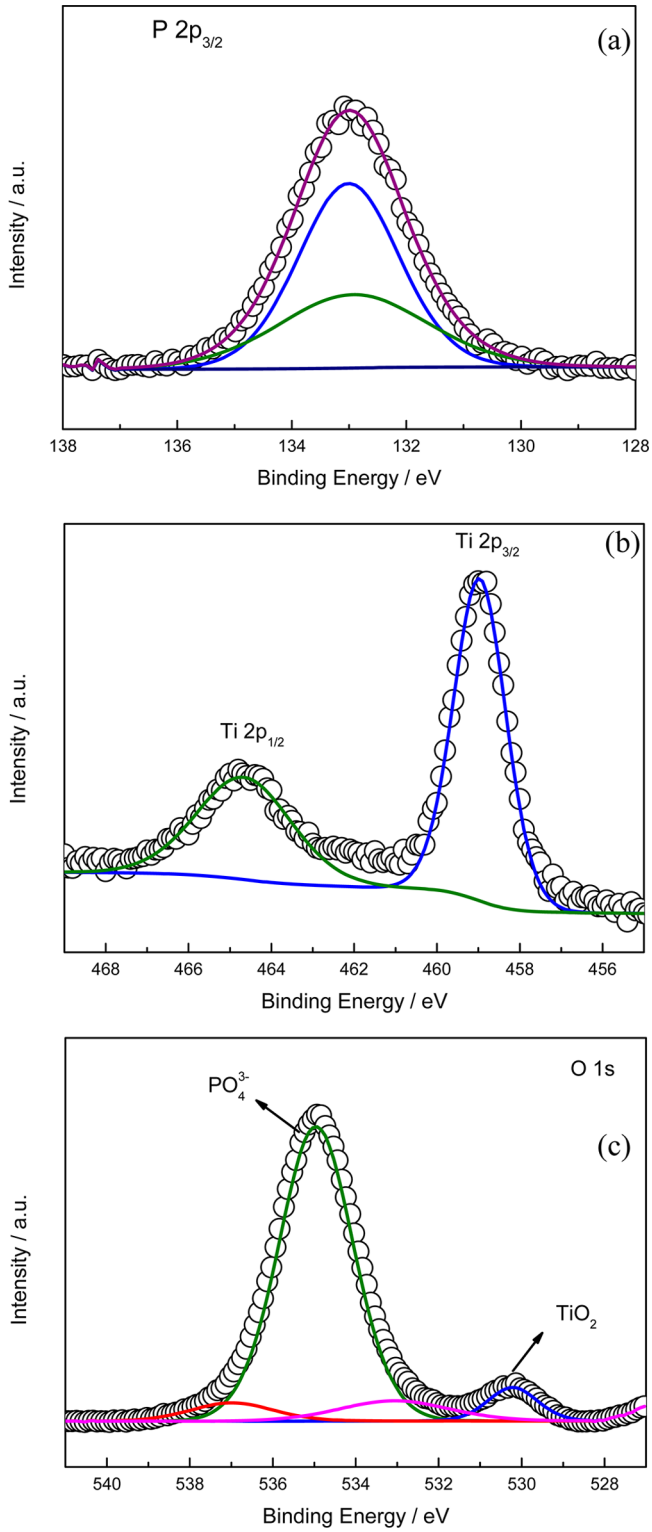

Figure 5. XPS spectra of Li_3PO_4: (a) P 2p, (b) Ti 2p, and (c) O 1s.

capacity is normalized by volumetric value according to the length of the nanotubes.

The insertion of Li^+ into anatase is known to be accompanied by a phase transition from tetragonal TiO_2 (space group $I4_1/amd$) to orthorhombic $Li_{0.5}TiO_2$ (space group *Imma*), whose reaction equation is expressed as follows:

$$TiO_2 + xLi^+ + xe^- \rightleftarrows Li_xTiO_2 \quad (1)$$

dx.doi.org/10.1021/am500189h | ACS Appl. Mater. Interfaces 2014, 6, 5669−5678

In this reaction equation, x is the amount of inserted Li^+ in the TiO_2, which is dependent on the crystal structure, anatase, rutile, or amorphous, and the microstructure of the materials used.[5,6,18,30] Figures S.I.9, Supporting Information, and 6 show

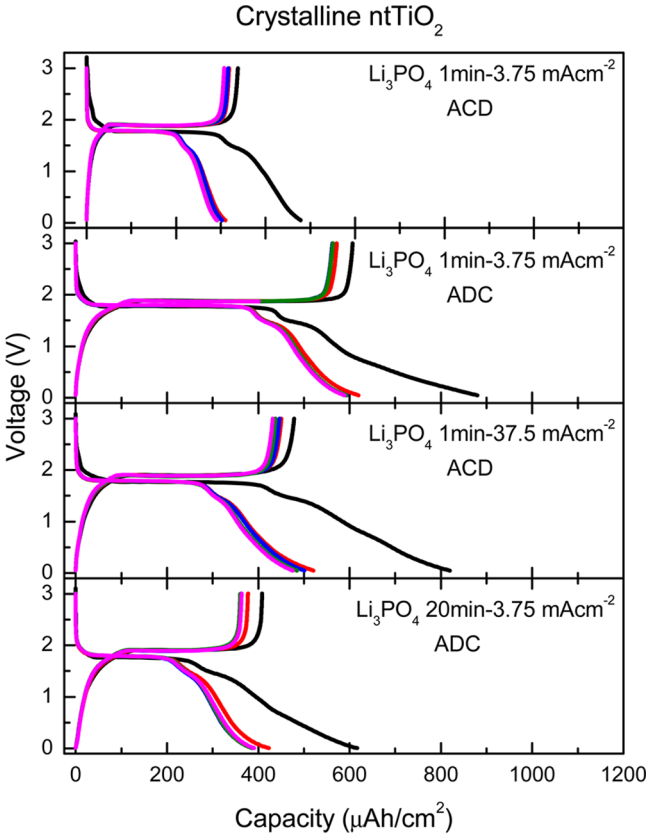

Figure 6. Galvanostatic discharge/charge curves of crystalline $ntTiO_2$ with deposited Li_3PO_4 after calcining (ACD) and before calcining (ADC). The voltage window is between 0.05−3.0 V using a rate of 50 μA cm^{-2}.

the first discharge−charge cycles of Li_3PO_4-coated $ntTiO_2$ cycled between 0.05−3.0 V for X-ray amorphous and X-ray crystalline anatase nanotubes, respectively. For amorphous $ntTiO_2$ no plateau is observed in the selected potential windows, but one pseudo-plateau at about 1.1−1.2 V contributes to a large irreversible capacity. Recently, Xiong et al. found by synchrotron X- ray spectroscopies and computational techniques the formation of a new crystalline material with high degree of symmetry in which Ti and Li are randomly distributed among all octahedral sites in a nearly ideal cubic closed packed oxygen array occurring principally for amorphous titania nanotubes between 1.25−0.9 V range.[31] The total capacity in the first discharge for Li_3PO_4-free $ntTiO_2$ electrode is about 993 μA h cm^{-2} (117−124 μA h cm^{-2} μm^{-1}) and the reversible capacity in first cycle is 535 μA h cm^{-2} (63−66 μA h cm^{-2} μm^{-1}), resulting in an efficiency of 54%. When depositing a thick layer of β−Li_3PO_4 (if 20 min and 37.5 mA cm^{-2} are used for deposition) covering the nanotubes, the electrochemical response resulted in an unwanted behavior because the first reversible capacity is reduced to 170 μA h cm^{-2} (20 μA h cm^{-2} μm^{-1}) and poor capacity retention is observed. Interestingly, the $ntTiO_2$ with a finely dispersed β−Li_3PO_4 deposit showed good electrochemical performance in terms of a higher reversible capacity (Supporting Information Figure S.I. 9a) and better cycling stability, 1000 μA h cm^{-2} (125 μA h cm^{-2} μm^{-1}) of first reversible capacity and 57% of reversibility, as compared to Li_3PO_4-free $ntTiO_2$ electrode. So, the conclusion is that in amorphous nanotubes, Li_3PO_4 can improve the cycling stability but there is no drastic change in the mechanism of the reactions in terms of polarization. From these results, the irreversible capacity is strongly dependent on the structure of $ntTiO_2$.

The mechanism of reaction is different for crystalline $ntTiO_2$ on which Li_3PO_4 can be deposited either after calcining (ACD) or before calcining (ADC) of the nanotubes. For crystalline samples we have performed the cycling experiments under two different voltage windows: (i) 0.05−3.0 and (ii) 1.0−3.0 V, see Figures 6 and 7, respectively. The discharge and charge plateau of Li_3PO_4-free $ntTiO_2$ samples were at approximately 1.75 and 1.9 V, respectively. The total capacity is 400 μA h cm^{-2} (48 μA

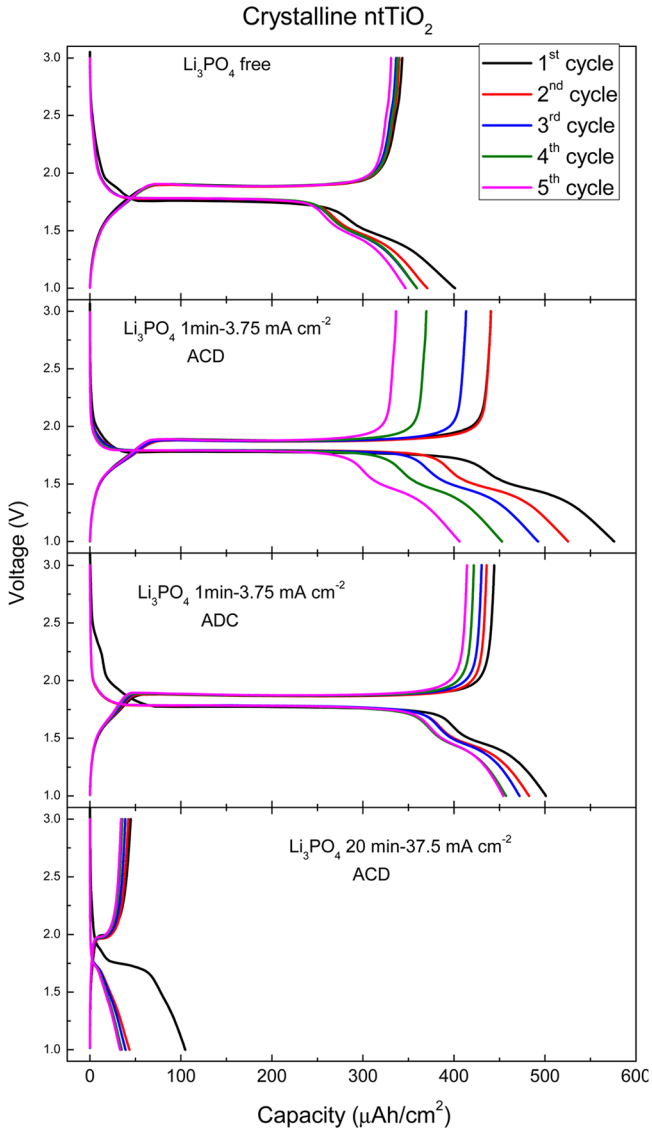

Figure 7. Recorded galvanostatic discharge/charge curves showing the effects of β-Li_3PO_4 and γ-Li_3PO_4 deposited on crystalline $ntTiO_2$. Please take into account that for obtaining β-Li_3PO_4 the $ntTiO_2$ were firstly calcined (named as ACD) and for obtaining γ-Li_3PO_4 everything is calcined together (named as ADC). A voltage window between 1.0−3.0 V using a rate of 50 μA cm^{-2} were selected.

dx.doi.org/10.1021/am500189h | ACS Appl. Mater. Interfaces 2014, 6, 5669−5678

h cm^{-2} μm^{-1}) and the first reversible capacity is 362 μA h cm^{-2} (42 μA h cm^{-2} μm^{-1}), with an efficiency of about 90 %. After electrodepositing lithium phosphate on the nanotubes two important changes in capacity value and polarization are observed. For instance, for β-Li_3PO_4/$ntTiO_2$ and γ-Li_3PO_4/$ntTiO_2$ samples deposited 1 min at 3.75 mA cm^{-2} a discharge/charge plateaus are observed at 1.78 and 1.86 V, which is ~0.1 V lower in energy as compared with uncoated samples. Moreover, the total capacity delivered by β-Li_3PO_4/$ntTiO_2$ and γ-Li_3PO_4/$ntTiO_2$ were about 576 and 500 μA h cm^{-2}, and the first reversible capacities were 525 and 482 μA h cm^{-2}, respectively. Thus, the efficiency from first to second cycle was about 91% and 96% , respectively. On the contrary, when using a thicker layer of Li_3PO_4 (20 min deposition) a very bad electrochemical performance expressed in terms of low capacity value (<50 μA h cm^{-2}) and high polarization (discharge/charge plateau at 1.74 and 2.0 V) of 0.26 V are observed.

Globally, the discharge curve behavior of the samples could be divided into three regions. The first region is a decrease in open-circuit voltage from 3 to 1.78 V. This region generally represented the formation of a solid solution.[32−34] Reduction of the anatase particle size resulted in a greater solubility of the Li^+ ions and a wider solid solution range.[33] The second region is recognized by a plateau at a voltage of approximately 1.78 V. It represents the two phase reaction of the insertion of Li^+ into half of the available interstitial octahedral sites of anatase. So, half of Ti^{4+} is turned into Ti^{3+} with the insertion of Li^+. Evidently, the length of the two phase reaction plateau depends on the amount of Li^+ inserted into bulk anatase, but also on the amount and shape of Li_3PO_4 coating. This fact is further corroborated for samples $ntTiO_2$ + Li_3PO_4 deposited 1 min denoted as ACD and ADC in Fig. 7. When comparing with uncoated samples, the third region can be recognized as an oblique line of dropping voltage from 1.75 to 1 V (Fig. 6), or from 1.75 to 0.05 V in the case of using wider voltage window. Sometimes the latter voltage range would provide high capacity initially, but is prejudicial to maintain the cycling stability. For this reason crystalline samples are cycled using narrower voltage window, to avoid loss of capacity and enhance efficiency. Others reason why a high irreversible capacity is observed in such material may be attributed to different phenomena. First, the formation of a very thin disordered layer at the electrode surface that may appear on both amorphous and crystalline electrodes.[5,6,35] Second, the irreversible reaction of Li^+ with adsorbed water molecules on the $ntTiO_2$ electrode.[36] Water and OH^- groups could be still present in some proportion in calcined samples, because the calcining temperature is not high enough to completely remove strongly chemisorbed water or bound water.[5,37] The difference in the irreversible capacity can be explained by the fact that a calcining treatment removes structural and chemical defects in the amorphous phase that act as Li^+ ion traps.[5]

Capacity retention has been studied during the first 100 cycles. The effect of different β-Li_3PO_4 coatings on amorphous TiO_2 during cycling is depicted in Figure 8a. The uncoated nanotubes exhibits a decay of reversible capacity from 535 to 100 μA h cm^{-2} over 60 cycles entailing a 19 % of efficiency. An enhanced performance is obtained for those electrodes based on $ntTiO_2$ + β-Li_3PO_4 fabricated during short deposition time, but outstand that of short deposition current. Thus, a maximum reversible capacity of 1000 μA h cm^{-2} (125 μA h cm^{-2} μm^{-1}) and retention of 300 μA h cm^{-2} (38 μA h cm^{-2} μm^{-1}) over 100 cycles is achieved for $ntTiO_2$ + β-Li_3PO_4 (Figure 8a) for 0.01−3.0 V voltage window. Using the same conditions, the uncoated crystalline $ntTiO_2$ had exhibited a poor electrochemical performance that in terms of capacity is resumed as 493, 335, and 20 μA h cm^{-2} recorded in first discharge (include reversible and irreversible reactions), first reversible discharge and after 100 cycles (Figure 8b), respectively. An improved electrochemical behavior when coating with β- and γ-Li_3PO_4 is observed. The latter treatment allowed obtaining very high initial capacity during the first 20 cycles since the capacity oscillated between 600−400 μA h cm^{-2}, but after 100 cycles the capacity decreased constantly to about 70 μA h cm^{-2}. However, one of the best electrochemical performances was found in crystalline $ntTiO_2$ + β-Li_3PO_4 because not only retained the

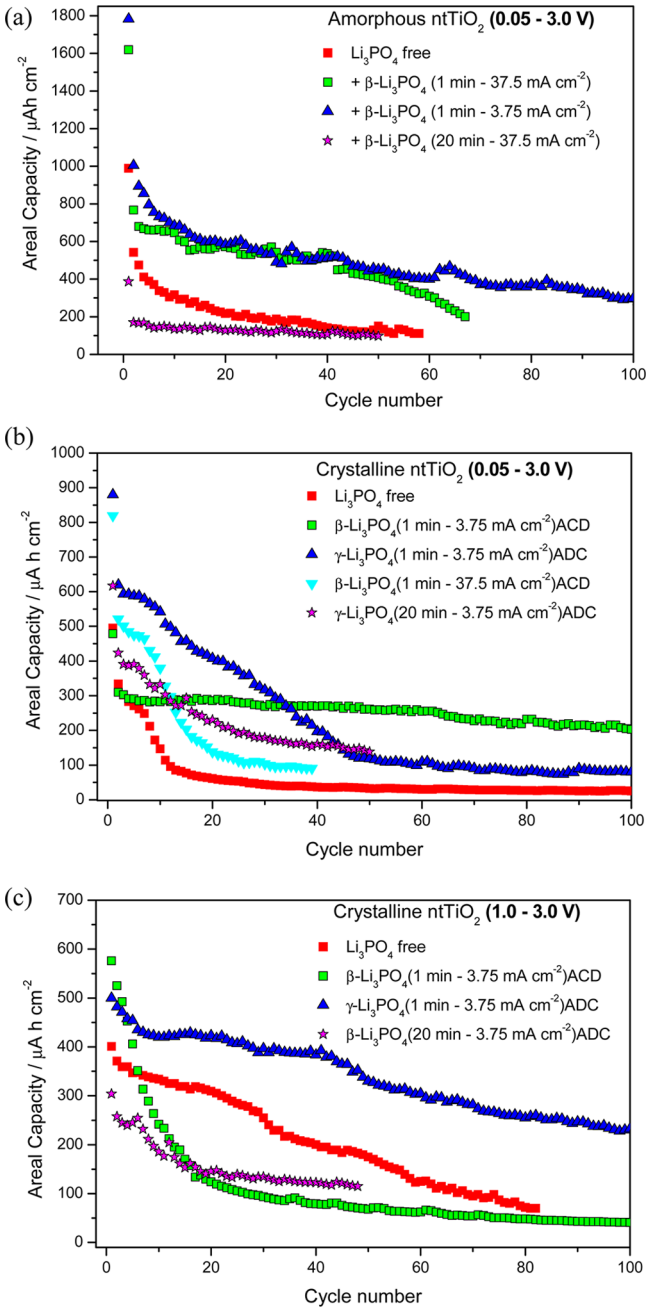

Figure 8. Cycle performances of the half cell batteries; (a) amorphous $ntTiO_2$ with β-Li_3PO_4 cycled between 0.01−3.0 V, (b) crystalline $ntTiO_2$+β-Li_3PO_4 or +γ-Li_3PO_4 cycled between 0.01−3.0 V, and (c) crystalline $ntTiO_2$+β-Li_3PO_4 or +γ-Li_3PO_4 cycled between 1.0−3.0 V.

dx.doi.org/10.1021/am500189h | ACS Appl. Mater. Interfaces 2014, 6, 5669−5678

capacity over 200 μA h cm^{-2} over 100 cycles but also initial capacity was moderately as high as 315 μA h cm^{-2}. If the voltage window is reduced from 0.05−3.0 to 1.0−3.0 V a different cycling behavior would be expected since we are avoiding reactions in the tail observed between 0.05−1.0 V mainly because of irreversible lithium trapped on defect sites and SEI formation. Figure 8c shows the proof that improving performance is possible when γ-Li_3PO_4 is in-situ-formed on the ntTiO_2 array. This sample exhibit the best electrochemical behavior using 1−3.0 V voltage window with a capacity of 500, 482, and 235 μA h cm^{-2} for first discharge, first reversible discharge, and over 100 cycles, respectively. It is good because avoid loss of irreversible capacity as using wider voltage window and may be no affected by electrolyte decomposition. We have seen that ntTiO_2 array + γ-Li_3PO_4 is overcoming the capacity of uncoated sample or whatever other different coating. Anyway, a bad electrochemical performance was always observed for the thicker layer obtained with high deposition times. For instance, 20 min of electrodeposition of Li_3PO_4 on TiO_2 for both amorphous and crystalline samples is observed this phenomenon. The thick layer may increase the resistance for Li reaction pass. In summary, it is important to highlight that formation of either β- or γ-Li_3PO_4 onto crystalline ntTiO_2 can be achieved simply by simply electrolytic depositing lithium phosphate after or before calcining the titania nanotubes. The gamma phase represents the best coating and in the case of cycling between 1.0 and 3.0 V, a well stable capacity is achieved over 100 cycles.

It has been proven that small additions of Li_3PO_4 on ntTiO_2 can improved the cycling properties and reduce the polarization voltage during discharge/charge of the electrodes. As seen by impedance, the ionic conductivity is better for small amount of lithium phosphate as compared with thicker layer of Li_3PO_4. Preliminary results agree with that reported by Xiao et al. in which when the addition of 1% of Li_3PO_4 increased the ionic conductivity and decreased with further increase of Li_3PO_4.[38] Moreover, dispersed Li_3PO_4 can increase the surface Li^+ ion diffusion rate and then increase the rate capacity as also found in $LiFePO_4$.[39]

The "rocking chair" battery developed in this work is based on the combination of ntTiO_2/γ-Li_3PO_4 negative electrode with a $LiFePO_4$ positive electrode. The fabrication of the former has been studied in detail in this work. $LiFePO_4$ is a well-known material with useful properties when used as electrode in lithium cells, including the negligible volume changes during cycling and an operating voltage outing comprised within the electrochemical windows of most widespread electrolytes.[6,18,23,40,41] If TiO_2 is prepared with adequate and specially designed architecture and morphology, extended cycling may take place without inducing any electrolyte decomposition at relatively high rate (5C). For the cathode, a single pair of sharp oxidation and reduction peaks, ascribing to the two-phase reaction of the Fe^{3+}/Fe^{2+} redox couple (i.e., lithium insertion and extraction), can be clearly discerned if the material is cycled vs lithium.[14,39,42] For pristine $LiFePO_4$, the oxidation and reduction peaks occur at 3.5 and 3.3 V, respectively, with the polarization being ∼0.3 V. Then the overall reaction of the rocking-chair cell studied here can be written as

$$\text{nt}TiO_2/\gamma\text{-}Li_3PO_4 + LiFePO_4 \leftrightarrow Li_{1-x}FePO_4 + \text{nt}Li_xTiO_2/\gamma\text{-}Li_3PO_4 \quad (2)$$

As expected from their respective voltages, the combination of the above mentioned electrodes gives rise to a battery operating in the 1.5−2.0 V range. Figure 9a shows the voltage

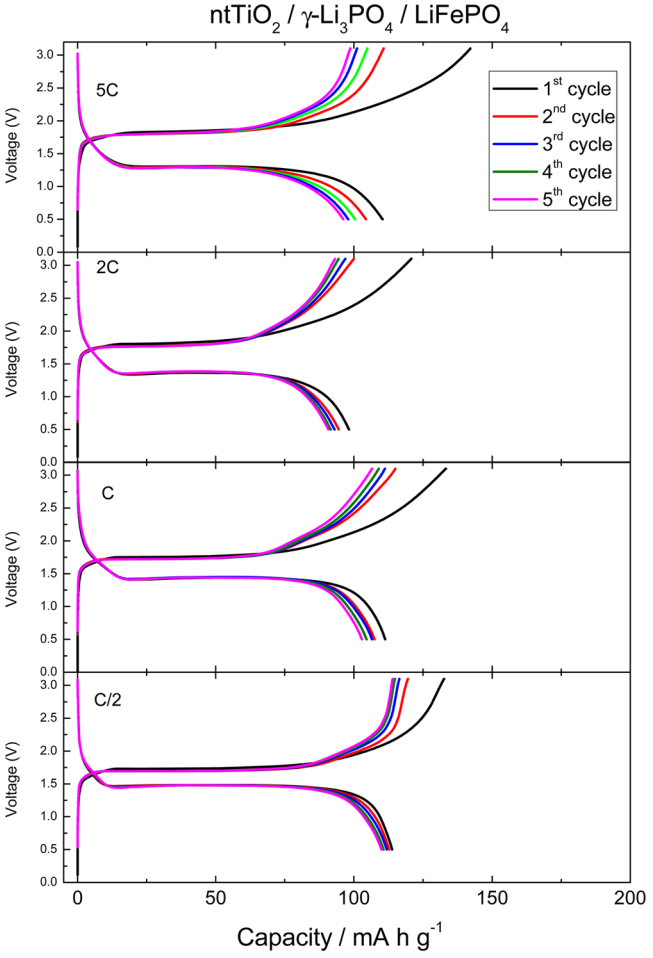

Figure 9. Performance of the ntTiO_2/γ-Li_3PO_4/$LiFePO_4$ rocking chair battery at various rates: 5C, 2C, C, C/2, and C/5. Shows the voltage profiles of the charge (lithium transfer from $LiFePO_4$ to ntTiO_2/γ-Li_3PO_4) and discharge (back transfer of lithium from ntTiO_2/γ-Li_3PO_4 to $LiFePO_4$). This combination gives rise to a battery operating in the 1.5−2.0 V range.

profiles of the charge (lithium transfer from $LiFePO_4$ to ntTiO_2/γ-Li_3PO_4)−discharge (back transfer of lithium from ntLi_xTiO_2/γ-Li_3PO_4 to $Li_{1-x}FePO_4$) cycles of the battery using 5C, 2C, C, C/2, and C/5 rate. It is worthy to note that both the very flat voltage profile centered on 1.7 V and the very small hysteresis between charge and discharge behavior during cycling effect are concrete evidences of high reversibility and relatively fast kinetic, specially that found stable (or with no significant change) at 2C. In addition, the battery was cycled at a maximum of 55 °C, and compared very favorably vs. that of room temperature as deduced from galvanostatic curves in terms of minimal polarization (0.1 V less) and slightly higher reversible capacity up to 160 and 130 mA h g^{-1} in charge and discharge, respectively (see Supporting Information Figure S.I.10). The battery, in fact, could be cycled at 5C, 2 C, 1C, C/2, and C/5 rate with 110, 98.5, 112, 114, and 120 mA h g^{-1} capacity delivery, that is, at a value not to far to the theoretical one, having in mind that the battery is cathode limited. These experiments have been also extended using long cycle number.

dx.doi.org/10.1021/am500189h | ACS Appl. Mater. Interfaces 2014, 6, 5669−5678

Thus, cycle life is relatively good in terms of capacity retention when using fast kinetics especially at > C rates. For instance, just after 50 cycles the full cell cycled at 2 C exhibited 85 mA h g^{-1} of capacity which is higher than that of the cell cycled at C/2 (75 mA h g^{-1}). At 5C the capacity retention is better than for slower scan rates over 190 cycles. Figure 10a shows a life

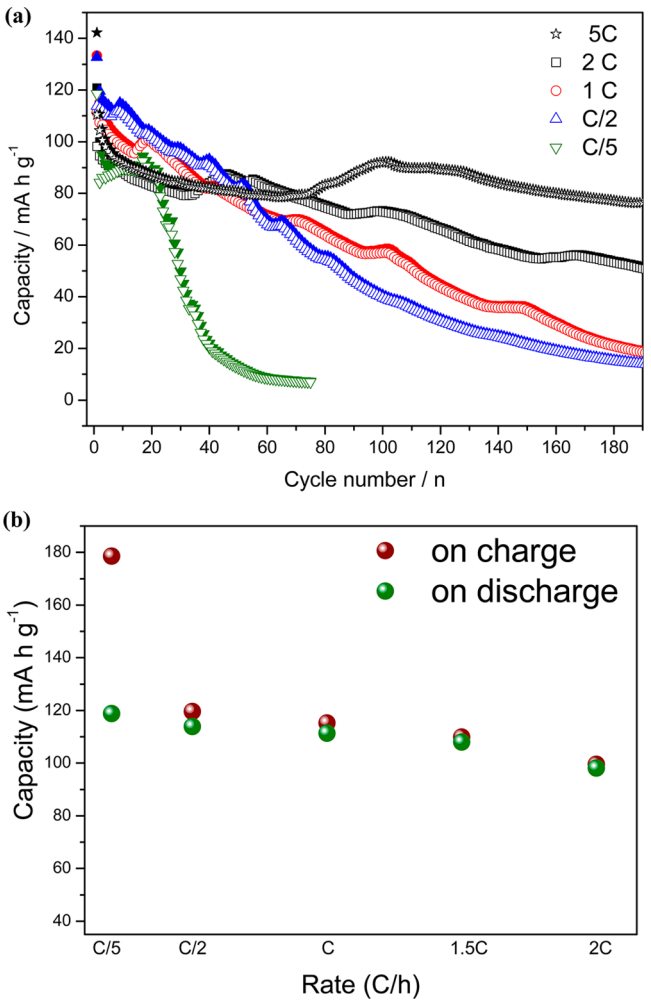

Figure 10. (a) Capacity delivery vs cycle number of the rocking chair battery cycled at 2C, C, C/2, and C/5 and (b) rate performance measured at room temperature.

extending, and over 190 cycles we have achieved capacity of 82, 68, and 45 mA h g^{-1} for 5C, 2C and C rates, respectively. This data evidence the high capability that can be achieved in our designed battery (Fig. 10b). A design towards high power battery is becoming realistic. It is considered that the Li_3PO_4 may play a role in enhancing surface stability of $ntTiO_2$ and $LiFePO_4$. Surface structural changes during electrochemical reaction deserve further investigation in the light of the electrochemical results presented here, but due to the problem that X-ray diffraction cannot offer any information, maybe another technique should be envisaged in the future to understand the exact role of the very thin layer of lithium phosphate. Undoubtly, the improved cycling performance is due to the well formed Li_3PO_4 layer on the $ntTiO_2$ array allowing high Li ionic diffusion rates as in lithium tin phosphates.[24]

CONCLUSIONS

Some important clues for preparing nanostructured electrodes based on surface modification of $ntTiO_2$ with γ-Li_3PO_4 are presented. Different possibilities have been explored to get optimum negative electrode and full microbattery. Apparently the use of 1 min and 3.75 $\mu A\ cm^{-2}$ are the optimum parameters to achieve γ-Li_3PO_4 coating on the entire $ntTiO_2$ array. The performance of the $ntTiO_2/\gamma$-Li_3PO_4 ($LiPF_6$ in EC:DEC)/$LiFePO_4$ rocking-chair microbattery delivered a maximum capacity of 110 mA h g^{-1} at 5C rate when imposing a cathode-limited active mass ratio to the electrodes. The obtained low-voltage microbattery (<2.0 V) could fit to applications demanding small-scale electrical power. By comparing capacity under different rates, it is shown that better capacity retention can be obtained at 5 C rate as compared with lower rates. The methodology presented for fabricating nanoarchitectured electrodes can be considered cheap and easy from the industrial point of view. The scalability of the experimental procedures presented in this work may be easily implemented for eventual commercial battery applications.

ASSOCIATED CONTENT

Supporting Information

PXRD patterns of β-Li_3PO_4, γ-Li_3PO_4, and $ntTiO_2/Li_3PO_4$ samples obtained under different electrochemical conditions in which unit cell parameters were adjusted. GISAXRD and XPS deep profile for $ntTiO_2/Li_3PO_4$ sample obtained for low deposition times. SEM images of electrodeposited Li_3PO_4 on Ti foils and on $ntTiO_2$ nanotubes. Galvanostatic curves of amorphous $ntTiO_2/\beta$-Li_3PO_4 in half cells, and galvanostatic curves of the rocking chair $ntTiO_2/\gamma$-$Li_3PO_4/LiFePO_4$ cycled at room temperature and at 55 °C. This material is available free of charge via the Internet at http://pubs.acs.org.

AUTHOR INFORMATION

Corresponding Author

*E-mail: q72maorg@uco.es. Tel.: +34 957 2186 37.

Notes

The authors declare no competing financial interest.

ACKNOWLEDGMENTS

The authors are indebted to MEC (MAT2011-22753) and "Junta de Andalucía" (FQM-288 and FQM-7206). G.F.O. is indebted to "Ramón y Cajal" program.

REFERENCES

(1) Vetter, J.; Novák, P.; Wagner, M. R.; Veit, C.; Möller, K.-C.; Besenhard, J. O.; Winter, M.; Wohlfahrt-Mehrens, M.; Vogler, C.; Hammouche, A. Ageing Mechanisms in Lithium-Ion Batteries. *J. Power Sources* **2005**, *147*, 269−281.

(2) Cherian, C. T.; Sundaramurthy, J.; Reddy, M. V.; Kumar, P. S.; Mani, K.; Pliszka, D.; Sow, C. H.; Ramakrishna, S.; Chowdari, B. V. R. Morphologically Robust $NiFe_2O_4$ Nanofibers as High Capacity Li-Ion Battery Anode Material. *ACS Appl. Mater. Interfaces* **2013**, *5*, 9957−9963.

(3) Bonino, F.; Busani, L.; Lazzari, M.; Manstretta, M.; Rivolta, B.; Scrosati, B. Anatase as a Cathode Material in Lithium-Organic Electrolyte Rechargeable Batteries. *J. Power Sources* **1981**, *6*, 261−270.

(4) Exnar, I.; Kavan, L.; Huang, S. Y.; Grätzel, M. Novel 2 V Rocking-chair Lithium Battery Based on Nano-crystalline Titanium Dioxide. *J. Power Sources* **1997**, *68*, 720−722.

(5) Ortiz, G. F.; Hanzu, I.; Djenizian, T.; Lavela, P.; Tirado, J.L.; Knauth, P. Alternative Li-Ion Battery Electrode Based on Self-Organized Titania Nanotubes. *Chem. Mater.* **2009**, *21*, 63−67.
(6) Ortiz, G.F.; Hanzu, I.; Lavela, P.; Knauth, P.; Tirado, J.L.; Djenizian, T. TiO_2 Nanotubes Manufactured by Anodization of Ti Thin Films for On-Chip Li-Ion 2D Microbatteries. *Electrochim. Acta* **2009**, *54*, 4262−4268.
(7) Ortiz, G.F.; Hanzu, I.; Lavela, P.; Knauth, P.; Tirado, J.L.; Djenizian, T. Nanoarchitectured TiO_2/SnO: A Future Negative Electrode for High Power Density Li-Ion Microbatteries? *Chem. Mater.* **2010**, *22*, 1926−1932.
(8) Ortiz, G.F.; Hanzu, I.; Lavela, P.; Tirado, J.L.; Knauth, P.; Djenizian, T. A Novel Architectured Negative Electrode Based on Titania Nanotube and Iron Oxide Nanowire Composites for Li-Ion Microbatteries. *J. Mater. Chem.* **2010**, *20*, 4041−4046.
(9) Bates, J. B.; Dudney, N. J.; Gruzalski, G. R.; Zuhr, R. A.; Choudhury, A.; Luck, D. F.; Robertson, J. D. Fabrication and Characterization of Amorphous Lithium Electrolyte Thin-Films and Rechargeable Thin-Film Batteries. *J. Power Sources* **1993**, *43*, 103−110.
(10) Dudney, N. J. In *Lithium Batteries: Science and Technology*; Nazri, G. A.; Pistoia, G., Eds.; Kluwer Academic Pub.: Dordrecht, the Netherlands, 2004; Chapter 20, pp 623−642.
(11) Liu, H. C.; Yen, S. K. Electrolytic Li_3PO_4 Coating on Pt. *J. Power Sources* **2006**, *159*, 245−248.
(12) Chung, S. Y.; Bloking, J. T.; Chiang, Y. M. Electronically Conductive Phospho-olivines as Lithium Storage Electrodes. *Nat. Mater.* **2002**, *1*, 123−128.
(13) Burba, C. A.; Frech, R. Local Structure in the Li-Ion Battery Cathode Material $Li_x(Mn_yFe_{1-y})PO_4$ for $0 < x \leq 1$ and $y = 0.0$, 0.5, and 1.0. *J. Power Sources* **2007**, *172*, 870−876.
(14) León, B.; Vicente, C.P.; Tirado, J. L.; Biensan, P.; Tessier, C. Optimized Chemical Stability and Electrochemical Performance of $LiFePO_4$ Composite Materials Obtained by ZnO Coating. *J. Electrochem. Soc.* **2008**, *155*, A211−A216.
(15) Kishida, K. Microstructure and Electrochemical Properties of the HT-$LiCoO_2$/$La_{2/3-x}Li_{3x}TiO_3$ Solid Electrolyte Interfaces. *J. Mater. Res.* **2010**, *25*, 1583−1587.
(16) Kobayashi, E.; Plashnitsa, L.S.; Doi, T.; Okada, S.; Yamaki, J. Electrochemical Properties of Li Symmetric Solid-State Cell With NASICON-Type Solid Electrolyte and Electrodes. *Electrochem. Commun.* **2010**, *12*, 894−896.
(17) Kuwata, N.; Iwagami, N.; Tanji, Y.; Matsuda, Y.; Kawamura, J. Characterization of Thin-Film Lithium Batteries with Stable Thin-Film Li_3PO_4 Solid Electrolytes Fabricated by ArF Excimer Laser Deposition. *J. Electrochem. Soc.* **2010**, *157*, A521−A527.
(18) González, J. R.; Alcántara, R.; Nacimiento, F.; Ortiz, G. F.; Tirado, J. L.; Zhecheva, E.; Stoyanova, R. Long-Length Titania Nanotubes Obtained by High-Voltage Anodization and High-Intensity Ultrasonication for Superior Capacity Electrode. *J. Phys. Chem. C* **2012**, *116*, 20182−20190.
(19) Keffer, C.; Mighell, A.; Mauer, F.; Swanson, H.; Block, S. Crystal Structure of Twinned Low-Temperature Lithium Phosphate. *Inorg. Chem.* **1967**, *6*, 119−125.
(20) Wang, B.; Chakoumakos, B.C.; Sales, B.C.; Kwak, B.S.; Bates, J.B. Synthesis, Crystal-Structure, and Ionic-Conductivity of a Polycrystalline Lithium Phosphorus Oxynitride with the γ-Li_3PO_4 Structure. *J. Solid State Chem.* **1995**, *115*, 313−323.
(21) Ross Macdonald, J. In *Impedance Spectroscopy*; Ross Macdonald, J., Eds.; John Wiley & Sons: Hoboken, NJ, U.S.A., 1987; Chapter 4, pp 191−236.
(22) Yu, X.; Bates, J.B.; Jellison, G.E., Jr.; Hart, F.X. A Stable Thin-Film Lithium Electrolyte: Lithium Phosphorus Oxynitride. *J. Electrochem. Soc.* **1997**, *144*, 524−532.
(23) Nacimiento, F.; González, J. R.; Alcántara, R.; Ortiz, G. F.; Tirado, J. L. Improving the Electrochemical Properties of Self-Organized Titanium Dioxide Nanotubes in Lithium Batteries by Surface Polyacrylonitrile Electropolymerization. *J. Electrochem. Soc.* **2013**, *160*, A3026−A3035.
(24) Cui, W. J.; Yi, J.; Chen, L.; Wang, C. X.; Xia, Y. Y. Synthesis and Electrochemical Characteristics of NASICON-Structured $LiSn_2(PO_4)_3$ Anode Material for Lithium-Ion Batteries. *J. Power Sources* **2012**, *217*, 77−84.
(25) Franke, R.; Chasse, Th.; Streubel, P.; Meisel, A. Auger Parameters and Relaxation Energies of Phosphorus in Solid Compounds. *J. Electron Spectrosc. Relat. Phenom.* **1991**, *56*, 381−388.
(26) Vidal-Abarca, C.; Lavela, P.; Ortiz, G.; Tirado, J. L. Electrochemical Performance of the Lithium Insertion in $Mn_{0.5-x}C_xTi_2(PO_4)_3$/C Composites ($x = 0$, 0.25, and 0.5) as Electrode Material for Lithium Batteries. *Electrochim. Acta* **2012**, *77*, 150−156.
(27) Silversmit, G.; De Doncker, G.; De Gryse, R. A Mineral TiO_2(001) Anatase Crystal Examined by XPS. *Surf. Sci. Spectra* **2002**, *9*, 21−29.
(28) Fleutot, B.; Pecquenard, B.; Martinez, H.; Letellier, M.; Levasseur, A. Investigation of the Local Structure of Lipon Thin Films to Better Understand the Role of Nitrogen on their Performance. *Solid State Ionics* **2011**, *186*, 29−36.
(29) Cserny, I.; Kövér, L.; Némethy, A.; Adachi, H.; Tanaka, I.; Sanjinés, R.; Coluzza, C.; Margaritondo, G. Realistic Cluster Approach for Interpreting the Valence-Band Structure of Phosphorus Oxyanions. *Surf. Interface Anal.* **1995**, *23*, 477−483.
(30) Saravanan, K.; Ananthanarayanan, K.; Balaya, P. Mesoporous TiO_2 with High Packing Density for Superior Lithium Storage. *Energy Environ. Sci.* **2010**, *3*, 939−948.
(31) Xiong, H.; Yildirim, H.; Shevchenko, E. V.; Prakapenka, V. B.; Koo, B.; Slater, M. D.; Balasubramanian, M.; Sankaranarayanan, S. K. R. S.; Greeley, J. P.; Tepavcevic, S.; Dimitrijevic, N. M.; Podsiadlo, P.; Johnson, C. S.; Rajh, T. Self-Improving Anode for Lithium-Ion Batteries Based on Amorphous to Cubic Phase Transition in TiO_2 Nanotubes. *J. Phys. Chem. C* **2012**, *116*, 3181−3187.
(32) Zakharova, G. S.; Jähne, C.; Popa, A.; Täschner, C.; Gemming, T.; Leonhardt, A.; Büchner, B.; Klingeler, R. Anatase Nanotubes as an Electrode Material for Lithium-Ion Batteries. *J. Phys. Chem. C* **2012**, *116*, 8714−8720.
(33) Gentili, V.; Brutti, S.; Hardwick, L. J.; Armstrong, A. R.; Panero, S.; Bruce, P. G. Lithium Insertion into Anatase Nanotubes. *Chem. Mater.* **2012**, *24*, 4468−4476.
(34) Jiang, C. H.; Wei, M. D.; Qi, Z. M.; Kudo, T.; Honma, I.; Zhou, H. S. Particle Size Dependence of the Lithium Storage Capability and High Rate Performance of Nanocrystalline Anatase TiO_2 Electrode. *J. Power Sources* **2007**, *166*, 239−243.
(35) Lindsay, M. J.; Skyllas−Kazacos, M.; Luca, V. Anodically Synthesized Titania Films for Lithium Batteries: Effect of Titanium Substrate and Surface Treatment. *Electrochim. Acta* **2009**, *54*, 3501−3509.
(36) Kim, J.; Cho, J. Rate Characteristics of Anatase TiO_2 Nanotubes and Nanorods For Lithium Battery Anode Materials at Room Temperature. *J. Electrochem. Soc.* **2007**, *154*, A542−A546.
(37) Shibata, T.; Zhu, Y.-C. Effect of Film Formation Conditions on the Structure and Composition of Anodic Oxide-Films on Titanium. *Corros. Sci.* **1995**, *37*, 253−270.
(38) Xiao, Z. B.; Chen, S.; Guo, M. M. Influence of Li_3PO_4 Addition on Properties of Lithium Ion-Conductive Electrolyte $Li_{1.3}Al_{0.3}Ti_{1.7}(PO_4)_3$. *Trans. Nonferrous Met. Soc. China* **2011**, *21*, 2454−2458.
(39) Zhao, S. X.; Ding, H.; Wang, Y. C.; Li, B. H.; Nan, C. W. Improving Rate Performance of $LiFePO_4$ Cathode Materials by Hybrid Coating of Nano-Li_3PO_4 and Carbon. *J. Alloys Compd.* **2013**, *566*, 206−211.
(40) Colbow, K. M.; Dahn, J. R.; Haering, R. R. Structure and Electrochemistry of the Spinel Oxides $LiTi_2O_4$ and $Li_{4/3}Ti_{5/3}O_4$. *J. Power Sources* **1989**, *26*, 397−402.
(41) Jiang, C.; Ichihara, M.; Honma, I.; Zhou, H. Effect of Particle Dispersion on High Rate Performance of Nano-Sized $Li_4Ti_5O_{12}$ Anode. *Electrochim. Acta.* **2007**, *52*, 6470−6475.
(42) Yao, J.; Wu, F.; Qiu, X.; Li, N.; Su, Y. Effect of CeO_2-Coating on the Electrochemical Performances of $LiFePO_4$/C Cathode Material. *Electrochim. Acta* **2011**, *56*, 5587−5592.